Rakenteiden Mekaniikka (Journal of Structural Mechanics)
Vol. 57, No. 3, 2024, pp. 80–98
https://rakenteidenmekaniikka.journal.fi/index
https://doi.org/10.23998/rm.143897

VERTAISARVIOITU
KOLLEGIALT GRANSKAD
PEER-REVIEWED
www.tsv.fi/tunnus

Extension of paperboard modelling with Föppl–von Kármán terms for improved stress state under suction pressure

M. Salo[1], J. Jokinen, M. Vilkko and M. Kanerva

Summary A practical method for solving the bending stiffness of a thin orthotropic plate based on measured deflection and known loading was studied. The target application was paperboard manufacturing and related process control. Here, finite element (FE) method was used to create virtual paperboard and its deflection data. The accuracy of the linear Kirchhoff plate model used in the practical method was tested against the FE model with known load and material properties. It was found that in the case of significant deflections, the linear Kirchhoff model was not accurate. The non-linear Föppl–von Kármán model takes into account the occurring membrane stresses and extends on the Kirchhoff model, allowing for larger deflection. The non-linear Föppl–von Kármán model was found to successfully describe the simulated situation and could be used to better solve for the paperboard's bending stiffness values over two axes.

Keywords: paper modelling, plate theory, finite element method, large deflection, reverse-engineering, bending stiffness

Received: 12 March 2024. Accepted: 23 August 2024. Published online: 1 October 2024.

Introduction

Plate models (e.g. Timoshenko [16]) are useful in predicting the behaviour of relatively thin plates under different loading scenarios and boundary conditions. In a typical scenario of mechanics, the plate's material and geometry are known while calculations are used to solve for unknown deformation and stresses occurring in the plate under certain loading and boundary conditions.

The Kirchhoff plate theory has been widely studied (e.g. Timoshenko [16], Wang [17], Bhaskar [2]) and is applicable to many cases of small deflections. The Föppl–von Kármán (FVK) theory, originally developed by Föppl [4] and von Kármán [9], extends upon the Kirchhoff theory, allowing the effects of the membrane stresses—typical of situations with significant deflection of a thin plate. Hakim [6] performed a literary review of the FVK plate theory about the stress distributions in a plate. The solving of the FVK equations analytically is very difficult and the validity of these equations has been questioned, e.g., by Ciarlet [3]. Lee [10] also discussed some problems of the theory, as well as some pitfalls in its practical application.

[1]Corresponding author: mikko.salo@tuni.fi

Paperboard and cardboard are anisotropic because of the fibrous nature (see e.g. Karakoç [8] and Niskanen [13]). However, due to the formation of machine made paperboard web, paperboard is often modeled using three orthogonal planes of symmetry: planes perpendicular to the machine direction, cross-machine direction and thickness direction (see e.g. Mäkelä [12], Marynowski [11], Garbowski [5]). The bending stiffness of paperboard is typically measured by mechanical tests conducted on test pieces after manufacturing (e.g. ISO 5628:2019 and TAPPI T 489), but this procedure is very slow for process control.

This work focuses on the development of a practical reverse-method that solves unknown material properties. The plate deformation, as well as its loading, are known (measured) and the goal is to solve for the plate's bending stiffnesses [14]. This methodology does not require knowledge about the boundary conditions, since the effect of boundary conditions are 'embedded' in the deformation field of the real world measurement.

We simulate a model of a supported paperboard plate using finite element model with capable solid elements and dense mesh. Thus, the inherent property scatter in real paperboard is excluded. When compared to the use of shell elements [15], a better solution of the in-plane stress-strain state is available in the thickness direction. Additionally, improved computation of the boundary condition with a contact is reached. In the new reverse-method, the finite element analysis (FEA) solution of deformations is processed fast (Matlab) similarly to the industrial target application. Especially the reverse-solved paperboard bending stiffness is studied in detail.

Plate modelling

Notation

We use the notation

$$(x, y, z) := (x_1, x_2, x_3) \tag{1}$$

for the Euclidean coordinate axes in $\mathbb{R}^3$ that describe the undeformed state of the plate. The displacement functions of the points in the material are

$$(u, v, w) := (u_1, u_2, u_3) : \mathbb{R}^3 \to \mathbb{R} \tag{2}$$

for x-, y- and z-directions respectively. The plate is assumed parallel to the xy-plane and its mid-surface[2] has $z = 0$ for all points. The material is assumed symmetric wrt. the mid-surface and the positive z-direction is chosen towards the deflection of the plate due to an external load distribution, q ($w > 0$).

Kinematic hypotheses

The kinematic hypotheses follow the bending of a plate, as written in many works (see for example [2]). The displacements u_i (for bending) are assumed to have the form

$$\begin{aligned} u_i &= u_i^0[x_1, x_2] - x_3 \frac{\partial u_3}{\partial x_i}, \quad i \in \{1, 2\} \\ u_3 &= u_3[x_1, x_2]. \end{aligned} \tag{3}$$

[2]We use "mid-surface" to refer to the middle surface of the plate in the thickness direction, as opposed to "middle of the plate", which refers to the middle area in the xy-plane.

Furthermore, it is assumed that the partial derivatives

$$\frac{\partial u_3}{\partial x_i}, \quad i \in \{1, 2\}$$

are significantly larger than any other partial derivative of the displacements; for the second powers it holds that

$$\frac{\partial u_k}{\partial x_i}\frac{\partial u_k}{\partial x_j} = 0 \quad \text{if } k \neq 3 \vee i = 3 \vee j = 3. \tag{4}$$

Strain-displacement relations

The finite strain-displacement relations are given according to the Green strain tensor [7]:

$$\epsilon_{ij} = \frac{1}{2}\left(\frac{\partial u_i}{\partial x_j} + \frac{\partial u_j}{\partial x_i} + \sum_{k=1}^{3}\frac{\partial u_k}{\partial x_i}\frac{\partial u_k}{\partial x_j}\right). \tag{5}$$

Applying equations 3 and 4, the approximate strains are

$$\hat{\epsilon}_{ij} = \epsilon^0_{ij}[x_1, x_2] - x_3\frac{\partial^2 u_3}{\partial x_i \partial x_j} \quad \text{if } i, j \in \{1, 2\} \tag{6}$$

where

$$\epsilon^0_{ij} = \frac{1}{2}\left(\frac{\partial u^0_i}{\partial x_j} + \frac{\partial u^0_j}{\partial x_i} + \frac{\partial u_3}{\partial x_i}\frac{\partial u_3}{\partial x_j}\right), \quad i, j \in \{1, 2\} \tag{7}$$

are called the membrane strains. We use the notation $\hat{\epsilon}$ to describe the approximate strain in the plate equation.

Moment equilibrium

The material in this study is assumed orthotropic and is described by nine elastic constants:

E_x, E_y, E_z,	elastic moduli
ν_{xy}, ν_{xz}, ν_{yz},	Poisson's ratios
G_{xy}, G_{xz}, G_{yz}	shear moduli

For the elastic moduli and Poisson's ratios, we use

$$\frac{\nu_{ij}}{E_i} = \frac{\nu_{ji}}{E_j}. \tag{8}$$

The bending stiffness of the orthotropic plate for the state given in 3 is defined as

$$D_x = \frac{E_x h^3}{12\eta}, \quad D_y = \frac{E_y h^3}{12\eta}, \quad D_{xy} = \frac{\nu_{xy} E_y h^3}{12\eta}, \tag{9}$$

where h is the (undeformed) thickness of the plate and

$$\eta = 1 - \nu^2_{xy}\frac{E_y}{E_x}. \tag{10}$$

The plate model here uses an approximation

$$\begin{aligned}\hat{\sigma}_{xx} &= \frac{1}{\eta}\big(E_x\hat{\epsilon}_{xx} + \nu_{xy}E_y\hat{\epsilon}_{yy}\big)\\ \hat{\sigma}_{yy} &= \frac{1}{\eta}\big(E_y\hat{\epsilon}_{yy} + \nu_{xy}E_y\hat{\epsilon}_{xx}\big)\\ \hat{\sigma}_{xy} &= 2G_{xy}\hat{\epsilon}_{xy}\end{aligned} \tag{11}$$

for the in-plane stresses. The notation $\hat{\sigma}$ describes the approximate stress in the plate equation. The moments per unit length are then defined as

$$\begin{aligned}m_x &:= \int_{-h/2}^{h/2} z\hat{\sigma}_{xx}\,dz = \int_{-h/2}^{h/2} \frac{z}{\eta}\big(E_x\hat{\epsilon}_{xx} + \nu_{xy}E_y\hat{\epsilon}_{yy}\big)\,dz\\ &= \underbrace{\frac{z^2}{2\eta}\big(E_x\epsilon^0_{xx} + \nu_{xy}E_y\epsilon^0_{yy}\big)}_{\text{evaluates to 0}} - \frac{z^3}{3\eta}\left(E_x\frac{\partial^2 w}{\partial x^2} + \nu_{xy}E_y\frac{\partial^2 w}{\partial y^2}\right)\Bigg|_{-h/2}^{h/2}\\ &= -D_x\frac{\partial^2 w}{\partial x^2} - D_{xy}\frac{\partial^2 w}{\partial y^2},\\ m_y &:= \int_{-h/2}^{h/2} z\hat{\sigma}_{yy}\,dz = \int_{-h/2}^{h/2} \frac{z}{\eta}\big(E_y\hat{\epsilon}_{yy} + \nu_{xy}E_y\hat{\epsilon}_{xx}\big)\,dz\\ &= -D_y\frac{\partial^2 w}{\partial y^2} - D_{xy}\frac{\partial^2 w}{\partial x^2},\\ m_{xy} &:= \int_{-h/2}^{h/2} z\hat{\sigma}_{xy}\,dz = \frac{G_{xy}h^3}{6}\frac{\partial^2 w}{\partial x\partial y}.\end{aligned} \tag{12}$$

For loads other than pure moment, an infinitesimally small volume ('element') of the plate experiences shear forces per unit length, Q_x and Q_y, in the positive z-direction, caused by the external load distribution, q. The situation is depicted in Figure 1.

Taking the sum of all the moments about the x- and y-axes (and disregarding the relatively small moments due to the load q, and due to the changes in Q_x and Q_y [16]), we have

$$\begin{aligned}Q_x &= \frac{\partial m_x}{\partial x} - \frac{\partial m_{xy}}{\partial y},\\ Q_y &= \frac{\partial m_y}{\partial y} - \frac{\partial m_{xy}}{\partial x}.\end{aligned} \tag{13}$$

Membrane stress relations

Let us define a stress funtion $F : \mathbb{R}^3 \to \mathbb{R}$ such that

$$\begin{aligned}\frac{\partial^2 F}{\partial x^2} &:= \frac{N_y}{h} := \hat{\sigma}_{yy}[x,y,0] = \frac{1}{\eta}\big(E_y\epsilon^0_{yy} + \nu_{xy}E_y\epsilon^0_{xx}\big)\\ \frac{\partial^2 F}{\partial y^2} &:= \frac{N_x}{h} := \hat{\sigma}_{xx}[x,y,0] = \frac{1}{\eta}\big(E_x\epsilon^0_{xx} + \nu_{xy}E_y\epsilon^0_{yy}\big)\\ \frac{\partial^2 F}{\partial x\partial y} &:= -\frac{N_{xy}}{h} := -\hat{\sigma}_{xy}[x,y,0] = -2G_{xy}\epsilon^0_{xy}.\end{aligned} \tag{14}$$

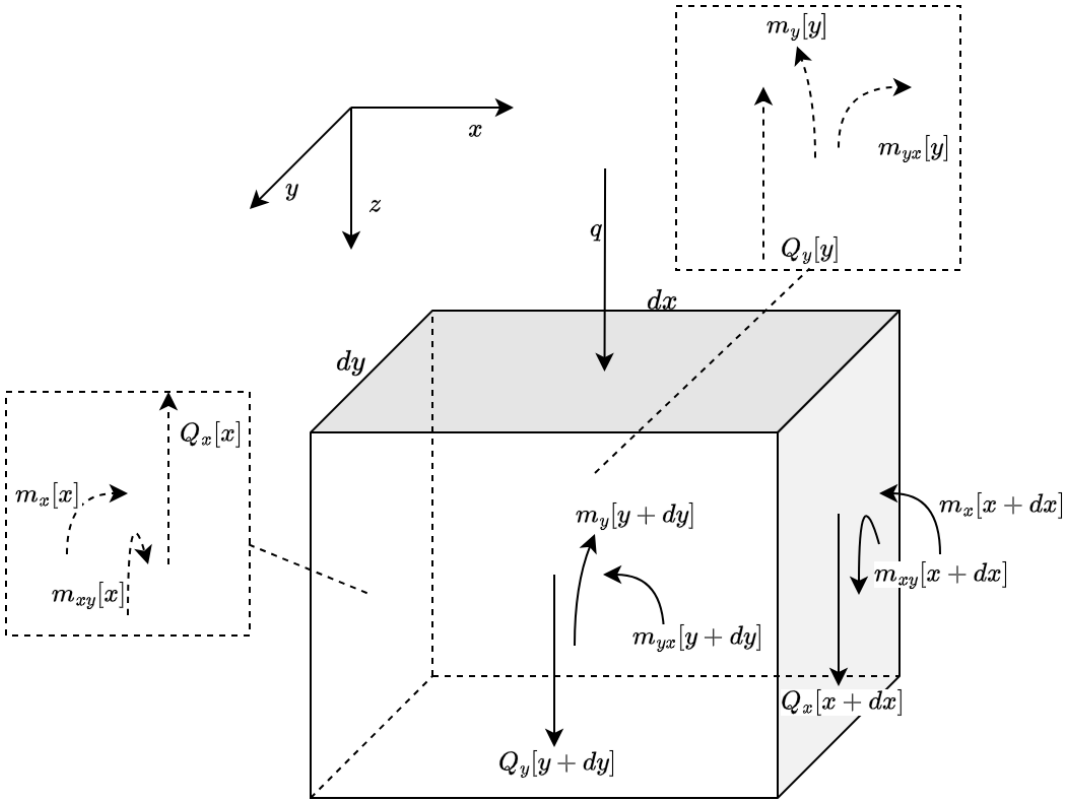

Figure 1: The forces and bending moments affecting a small plate element

For the equilibrium of resultant forces in the plane, it must hold that

$$\begin{aligned} \frac{\partial N_x}{\partial x} + \frac{\partial N_{xy}}{\partial y} &= 0 \\ \frac{\partial N_y}{\partial y} + \frac{\partial N_{xy}}{\partial x} &= 0. \end{aligned} \tag{15}$$

Equation 14 can be inverted to

$$\begin{aligned} \epsilon^0_{xx} &= \frac{1}{E_x}\frac{\partial^2 F}{\partial y^2} - \frac{\nu_{xy}}{E_x}\frac{\partial^2 F}{\partial x^2} \\ \epsilon^0_{yy} &= \frac{1}{E_y}\frac{\partial^2 F}{\partial x^2} - \frac{\nu_{xy}}{E_x}\frac{\partial^2 F}{\partial y^2} \\ \epsilon^0_{xy} &= -\frac{1}{2G_{xy}}\frac{\partial^2 F}{\partial x \partial y}. \end{aligned} \tag{16}$$

Taking the second partial derivatives of the membrane strains, summing, and applying equation 7, we have

$$\begin{aligned}
&\frac{\partial^2 \epsilon^0_{xx}}{\partial y^2} + \frac{\partial^2 \epsilon^0_{yy}}{\partial x^2} - 2\frac{\partial^2 \epsilon^0_{xy}}{\partial x \partial y} \\
&= \frac{\partial^3 u}{\partial x \partial y^2} + \frac{\partial^3 w}{\partial x \partial y^2}\frac{\partial w}{\partial x} + \left(\frac{\partial^2 w}{\partial x \partial y}\right)^2 \\
&+ \frac{\partial^3 v}{\partial x^2 \partial y} + \frac{\partial^3 w}{\partial x^2 \partial y}\frac{\partial w}{\partial y} + \left(\frac{\partial^2 w}{\partial x \partial y}\right)^2 \\
&- \frac{\partial^3 u}{\partial x \partial y^2} - \frac{\partial^3 v}{\partial x^2 \partial y} - \frac{\partial^3 w}{\partial x^2 \partial y}\frac{\partial w}{\partial y} - \frac{\partial^2 w}{\partial x^2}\frac{\partial^2 w}{\partial y^2} - \left(\frac{\partial^2 w}{\partial x \partial y}\right)^2 - \frac{\partial w}{\partial x}\frac{\partial^3 w}{\partial x \partial y^2} \\
&= \left(\frac{\partial^2 w}{\partial x \partial y}\right)^2 - \frac{\partial^2 w}{\partial x^2}\frac{\partial^2 w}{\partial y^2}.
\end{aligned} \tag{17}$$

On the other hand, substituting 16 into the first expression of 17, we have

$$\begin{aligned}
&\frac{\partial^2 \epsilon^0_{xx}}{\partial y^2} + \frac{\partial^2 \epsilon^0_{yy}}{\partial x^2} - 2\frac{\partial^2 \epsilon^0_{xy}}{\partial x \partial y} \\
&= \frac{1}{E_x}\frac{\partial^4 F}{\partial y^4} - \frac{\nu_{xy}}{E_x}\frac{\partial^4 F}{\partial x^2 \partial y^2} + \frac{1}{E_y}\frac{\partial^4 F}{\partial x^4} - \frac{\nu_{xy}}{E_x}\frac{\partial^4 F}{\partial x^2 \partial y^2} + \frac{1}{G_{xy}}\frac{\partial^4 F}{\partial x^2 \partial y^2}.
\end{aligned} \tag{18}$$

These together yield one of the FVK equations:

$$\frac{1}{E_y}\frac{\partial^4 F}{\partial x^4} + \frac{1}{E_x}\frac{\partial^4 F}{\partial y^4} + \left(\frac{1}{G_{xy}} - \frac{2\nu_{xy}}{E_x}\right)\frac{\partial^4 F}{\partial x^2 \partial y^2} = \left(\frac{\partial^2 w}{\partial x \partial y}\right)^2 - \frac{\partial^2 w}{\partial x^2}\frac{\partial^2 w}{\partial y^2}. \tag{19}$$

Transverse force equilibrium

By summing the total forces acting in z-direction in Figure 1, we have

$$-Q_x[x]\,dy + Q_x[x+dx]\,dy - Q_y[y]\,dx + Q_y[y+dy]\,dx + q\,dx\,dy = 0. \tag{20}$$

Applying the Taylor approximation as well, as equations 13 and 12, we arrive at the Kirchhoff plate equation [16]

$$D_x\frac{\partial^4 w}{\partial x^4} + H\frac{\partial^4 w}{\partial x^2 \partial y^2} + D_y\frac{\partial^4 w}{\partial y^4} = q, \tag{21}$$

where

$$H = 2D_{xy} + \frac{G_{xy}h^3}{3}. \tag{22}$$

Since the plate is deflected, the forces per unit length (N as defined in equation 14) also have a non-negative z-component proportional to the sine of the angle, α, between the plate's surface and the xy-plane. This component is depicted in Figure 2. The z-components of the resulting total forces affecting a small volume element are calculated using the Taylor approximation and small angle approximation as

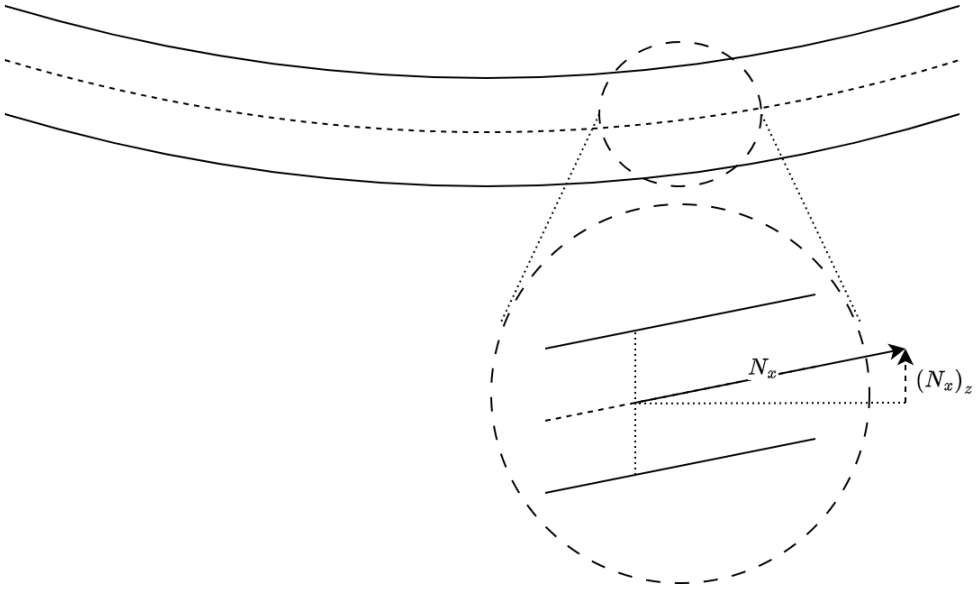

Figure 2: A view from the side of a bent plate depicting the z-component of the in-plane force per unit length N_x. This figure is an adaptation from the literature [16].

$$
\begin{aligned}
(N_x)_z &= \underbrace{-N_x\,dy}_{\text{force}[x]}\ \underbrace{\frac{\partial w}{\partial x}}_{\sin(\alpha[x])} + \underbrace{\left(N_x + \frac{\partial N_x}{\partial x}\,dx\right)dy}_{\text{force}[x+dx]\ \text{(Taylor)}}\ \underbrace{\left(\frac{\partial w}{\partial x} + \frac{\partial}{\partial x}\left(\frac{\partial w}{\partial x}\right)dx\right)}_{\sin(\alpha[x+dx])\ \text{(Taylor)}} \\
&= N_x\frac{\partial^2 w}{\partial x^2}\,dx\,dy + \frac{\partial N_x}{\partial x}\frac{\partial w}{\partial x}\,dx\,dy, \qquad (23)
\end{aligned}
$$

where we ignored all terms that included the third powers of the infinitesimally small lengths dx, dy. Similarly, we have

$$
\begin{aligned}
(N_y)_z &= N_y\frac{\partial^2 w}{\partial y^2}\,dx\,dy + \frac{\partial N_y}{\partial y}\frac{\partial w}{\partial y}\,dx\,dy \\
(N_{xy})_z &= 2N_{xy}\frac{\partial^2 w}{\partial x\partial y}\,dx\,dy + \frac{\partial N_{xy}}{\partial x}\frac{\partial w}{\partial x}\,dx\,dy + \frac{\partial N_{xy}}{\partial y}\frac{\partial w}{\partial y}\,dx\,dy. \qquad (24)
\end{aligned}
$$

Summing the expressions 23 and 24 while applying equation 15, and adding them to the total force in equation 20, we obtain the second FVK equation

$$
D_x\frac{\partial^4 w}{\partial x^4} + H\frac{\partial^4 w}{\partial x^2\partial y^2} + D_y\frac{\partial^4 w}{\partial y^4} = q + h\left(\frac{\partial^2 F}{\partial y^2}\frac{\partial^2 w}{\partial x^2} - 2\frac{\partial^2 F}{\partial x\partial y}\frac{\partial^2 w}{\partial x\partial y} + \frac{\partial^2 F}{\partial x^2}\frac{\partial^2 w}{\partial y^2}\right). \qquad (25)
$$

Equations 19 and 25 are called the Föppl-von Kármán equations for large deflection of plates.

Finite element model

A finite element model of a thin plate suspended over a support with a circular hole was analysed in Abaqus/Standard 2021 (Simulia). The model consists of two parts: A 30 mm × 30 mm plate with a thickness of 0.3 mm, and a rectangular support with a circular 23 mm (diameter) cut hole in the middle. The plate is set on top of the support. The modeled plate is a representation of thin paperboard, whereas the support is a representation of a relatively thick and rigid machined metal part with a cut hole. The

model geometry is illustrated in Figure 3. Rigid body motion constraints were introduced in one corner of the support, restricting all translations and rotations. No boundary conditions were given to the plate.

The plate-simulating paperboard is modeled as a homogeneous solid 3D-object. The material model is defined by nine engineering constants. The constants' values are shown in Table 1. The support is an isotropic homogeneous solid 3D-object, but is modeled analytically rigid since the support is assumed significantly stiffer than the plate.

The plate is meshed with uniform 0.15 mm cubic elements, which yields 200 elements in the width directions and two elements in the thickness direction. Uniform shape and size are used for convenience—to allow easy use of data in the reverse-method. With these choices, the thickness direction is also divided into three 'layers' of nodes (i.e. two 'layers' of elements), one of which is the mid-surface of the plate. This ensures that the analytical plate model and its membrane stresses can be compared to those of FE analysis. The elements of the plate are 3D-stress elements with quadratic geometric order (C3D20R). The support has less dense mesh (typical element dimension 1 mm) and is meshed by first (geometric) order elements. Its mesh is also not rectangular near the circular cut.

A uniform constant pressure difference (-1000 Pa) is applied to the nodes in the bottom of the plate in the area of the circular cut in the support, which simulates suction (negative pressure difference) in the real measurement system. The clamped boundary conditions are set by the corner of the support plate. The surface-to-surface contact was placed between the plate and the support. The node to surface discretization method and frictionless finite sliding formulation was used for the contact. Geometric nonlinearity was included in the model.

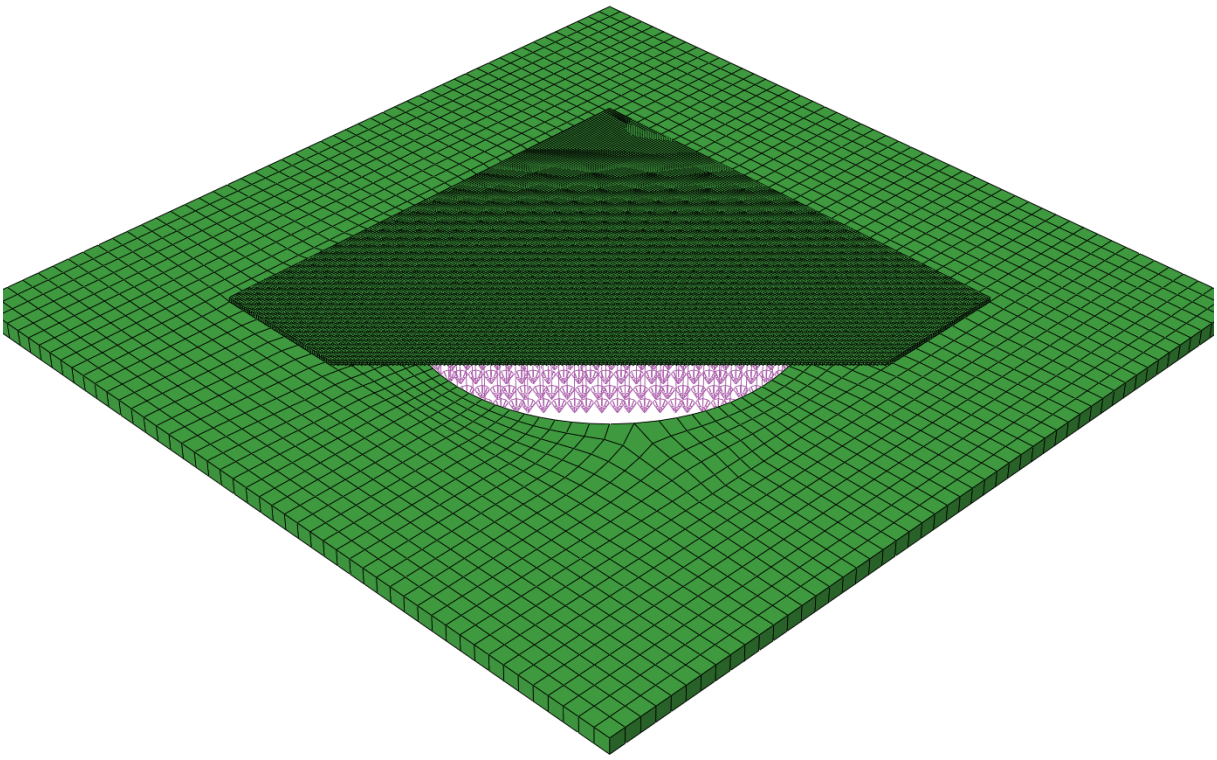

Figure 3: The meshing of the FE models. A portion of the plate has been removed for clarity.

Table 1: Material constants used in simulations. Units: 10^9 Pa, except Poisson's ratios are unitless. Source: [1]

Material	E_x	E_y	E_z	ν_{yz}	ν_{xz}	ν_{xy}	G_{yz}	G_{xz}	G_{xy}
Carton stock	7.44	3.47	0.040	0.021	0.008	0.15	0.099	0.137	2.04
Linerboard 90 lb	7.46	3.01	0.029	0.021	0.109	0.117	0.104	0.129	1.80

The reverse-method

The reverse-method for solving the paperboard's bending stiffness utilizes measured data from its deflection and the applied lateral load. Here, this measured data is represented by FE-simulated mid-surface deflection and the load used in the FE-model, respectively. The calculations are performed using Matlab scripts.

Firstly, the fourth order partial derivatives present in equation 21 are obtained by differentiating the discrete deflection data, w, using the central difference method, for example

$$\frac{\partial w}{\partial x}[x_n, y_m] = \frac{w[x_{n+1}, y_m] - w[x_{n-1}, y_m]}{x_{n+1} - x_{n-1}}, \tag{26}$$

recursively. The derivatives are also median and frequency filtered to remove noise.

Second, a calculation domain, Ω, is chosen by the operator and the calculated fourth partial derivatives and the known load (q) are used to form system of linear equations

$$D_x \frac{\partial^4 w}{\partial x^4}[x_n, y_m] + H \frac{\partial^4 w}{\partial x^2 \partial y^2}[x_n, y_m] + D_y \frac{\partial^4 w}{\partial y^4}[x_n, y_m] = q[x_n, y_m], \quad [x_n, y_m] \in \Omega \tag{27}$$

according to equation 21. The unknowns to be solved from this system are D_x, D_y and H. If the plate's thickness and stress state are also known (as in FE models), equation 25 may be used to form this system of linear equations by adding the additional terms to right sides of the equations.

Finally, the unknowns of the system are solved. The system has three unknowns and as many equations as there are data points in the chosen domain, hence least squares fitting is used. The domain is chosen such that the plate equations hold within it.

Results

Simulations were conducted with the FE-models and the deflection and inputs were used and compared to the ones given by the reverse-method. The following sections show the results using the "Carton stock"-material with its constants in Table 1. In essential consideration is the application of deflection data at the middle of plate, i.e., sufficiently far from strong effects by the boundary conditions (as modelled in FE).

Effect of approximations on the stress-distributions

The stress distributions according to the plate model's hypotheses were calculated and and compared to the stress distribution obtained from the FE analysis. The displacements

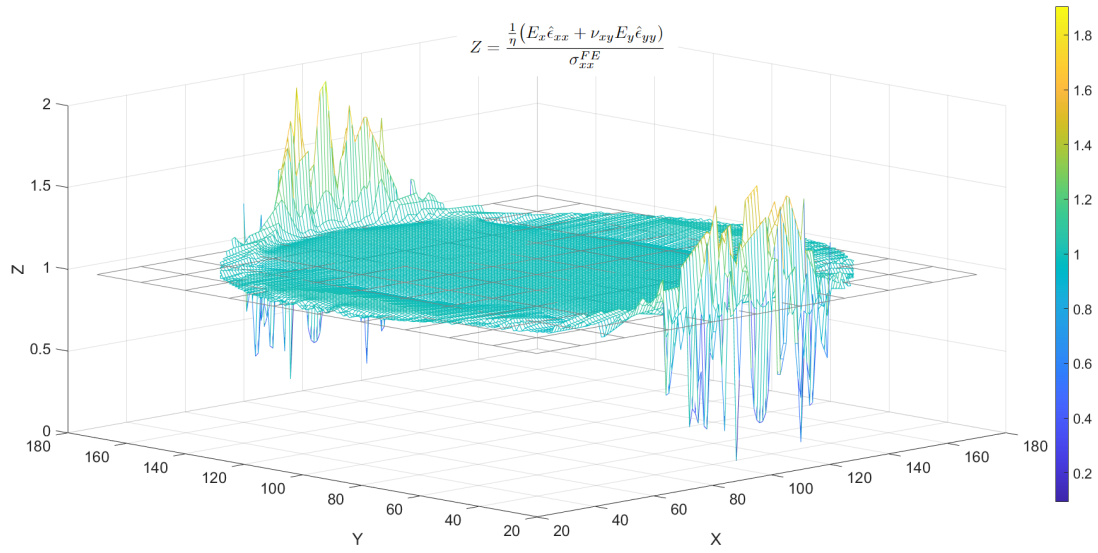

Figure 4: The mid-surface stress $\hat{\sigma}_{xx}$ calculated according to eqs. 11 and 6 divided by the corresponding FE-simulated one in the middle of the plate. Linear interpolation was used where the denominator is close to zero.

u_x^0, u_y^0 and w of the mid-surface, similarly, were used to calculate the strains $\hat{\epsilon}_{ij}$ according to equations 6 and 7 for each node in the model and for the comparison purpose. The stresses $\hat{\sigma}_{ij}$ were then calculated according to equation 11 using the same material constants as in the FE-model.

Figure 4 shows the results for the stress distribution in x-direction in the middle plane of the plate. The calculated and FE analysis values are in relatively good agreement, with the exception of the near-edge regime (nodes near the contact forces between the plate and its support). These results in the middle of the plate show, that the approximated stresses of the plate equation do not significantly differ from the stress distributions of the FE-model.

Similar results are obtained for the stresses in the top and bottom surfaces of the plate i.e. the stresses due to moments. The relative errors between the calculated and simulated stresses are around 1%–2% data points (nodes in FE mesh) reasonably far from the contact and regimes where the stress value is close to zero.

Accuracy of plate equations

The ability of the plate equations to represent the FE-model (its material model) was tested. Using the FE-simulated data, the external load q in equations 21 and 25 was resolved and compared to the (constant) pressure difference used in the FE simulation. The bending stiffnesses D_x, D_y and H were calculated from the engineering constants used in the FE material model according to equation 9. The thickness of the plate, h, was obtained from the initial part (FE-model). The partial derivatives of w come from differentiating the simulated mid-surface deflection, and the derivatives of the stress function F come from the simulated membrane stresses according to equation 14.

The classical Kirchhoff plate equation 21 was first tested. The resulting re-solved load distribution is shown in Figure 5. The loading is approximately the same as the -1000 Pa pressure difference used in the simulation. There are however large opposite sign loads in

the areas near the contact to the support. More interestingly, the calculated load near the center of the area (hole) is significantly different from the input of FE simulation. This suggests that the classical plate theory is insufficient to describe the plate bending in this scenario, which is supported by fact that the neglected membrane stresses are highest near the center of the plate, as was seen for example in Figure 4.

Figure 6 shows the re-solved loading using the FVK equation 25. The results match well the constant pressure value also at the center of the plate. The contact areas still exhibit behaviour not explained by the plate model.

The validity of equation 19 was also tested. The membrane stresses were differentiated, and the left and right sides of the equation were evaluated at the simulation data points and compared. The results of this comparison are shown in Figure 7. The equation 19 tends to be very accurate (in nodes) sufficiently far away from the contact.

Reverse-method for solving the plate's bending stiffnesses

The reverse-method for calculating the plate's bending stiffnesses, D_x, D_y and H, based on the FE-simulated deflection data was tested. We assumed that the deflection field w and external load q are known and that the different plate equations, 21 and 25, solve for the bending stiffnesses. In the case of FVK-equation, the stress fields were also assumed known.

The deflection was obtained from the FE simulated data and the (constant) external load from FE-model input. With these assumptions, we have a linear systems of equations where the unknowns are the plate's bending stiffnesses and each data point (i.e., each node in the plate's mid-surface) provides an equation. The domain in which we evaluate w and q determines the number of equations. We used both circular and ring-shaped domains with the same center point as in the hole. For this area, or domain, the radii ranged from 0 up to the radius of the hole. Examples of these are depicted in Figure 8. The plate's bending stiffnesses are then solved from the linear system of equations with least squares.

The solved bending stiffnesses as a function of the circular domain radius as well as the corresponding ones used in the FE-model are shown in Figure 9. The Kirchhoff equation fails to calculate the correct values using this method. However, the larger the domain radius, the closer to the actual values the calculated parameters are. This agrees with the fact that the Kirchhoff plate equation is more accurate far from the center of the plate as was seen in Figure 5. The effect can be alleviated using ring-shaped domains for the collection of FE-data as in Figure 10. Here, the data from the center of the plate is omitted for the outer domains, hence even the Kirchhoff equation is able to solve for the plate's bending stiffnesses. The FVK plate model solves the parameters more accurately, although it fails near the exact center as well. Both plate models fail to calculate the bending stiffnesses if data near the contact (boundary condition) is included.

Discussion

The validity of analytical plate equations of the reverse-method was tested using virtual paperboard deflection produced via FE-analysis. The scatter of material properties in a real-life application was omitted this way. In the application, the deflection of the plate and the external load applied are known at certain accuracy from specialized measurements. In this study, the use of FE-analysis also removed disturbances such as measurement noise and dynamic phenomena. Compared to the FE-modeling scenario, the real application also includes externally caused stresses in the plane of the plate, i.e. stresses

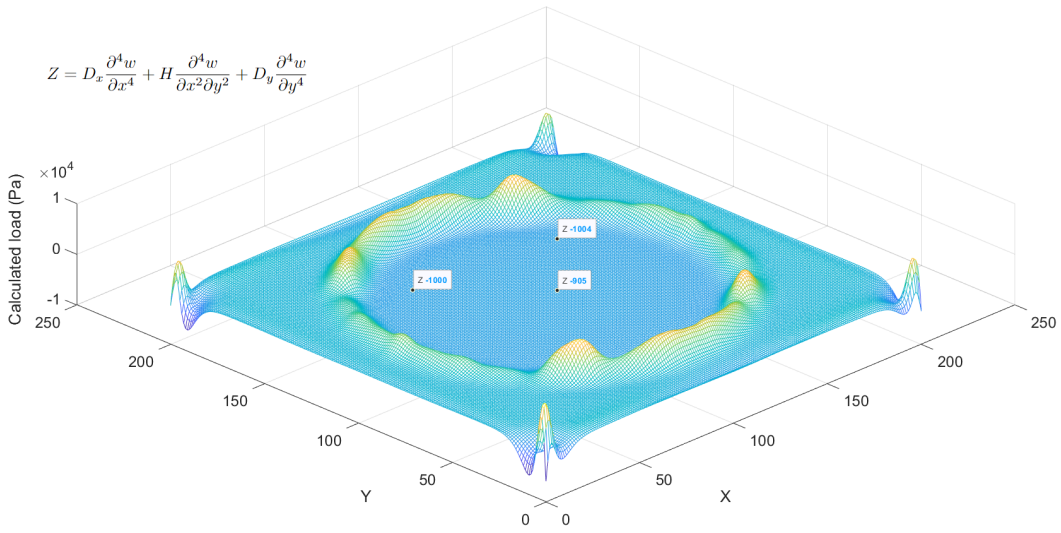

(a) The entire plate

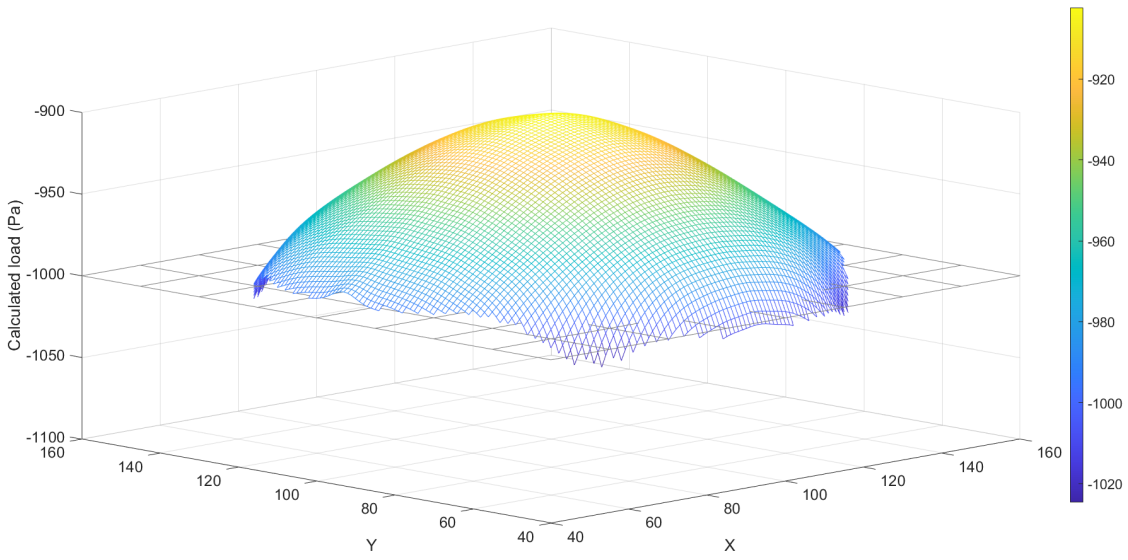

(b) Middle of the plate

Figure 5: The external load calculated according to the Kirchhoff plate equation using FE-model inputs and simulated data.

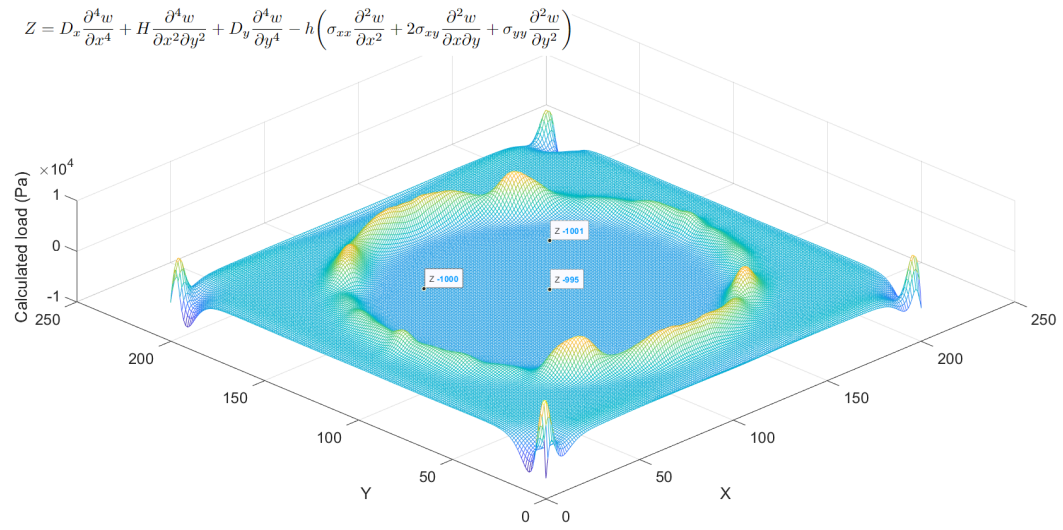

(a) The entire plate

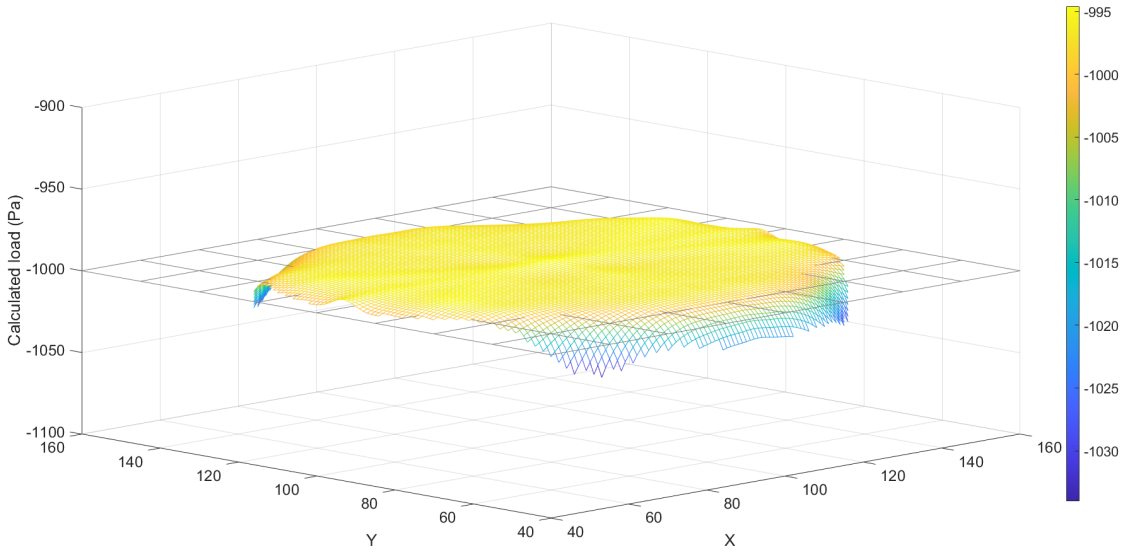

(b) Middle of the plate

Figure 6: The external load calculated according to the FVK plate equation using FE-model inputs and simulated data.

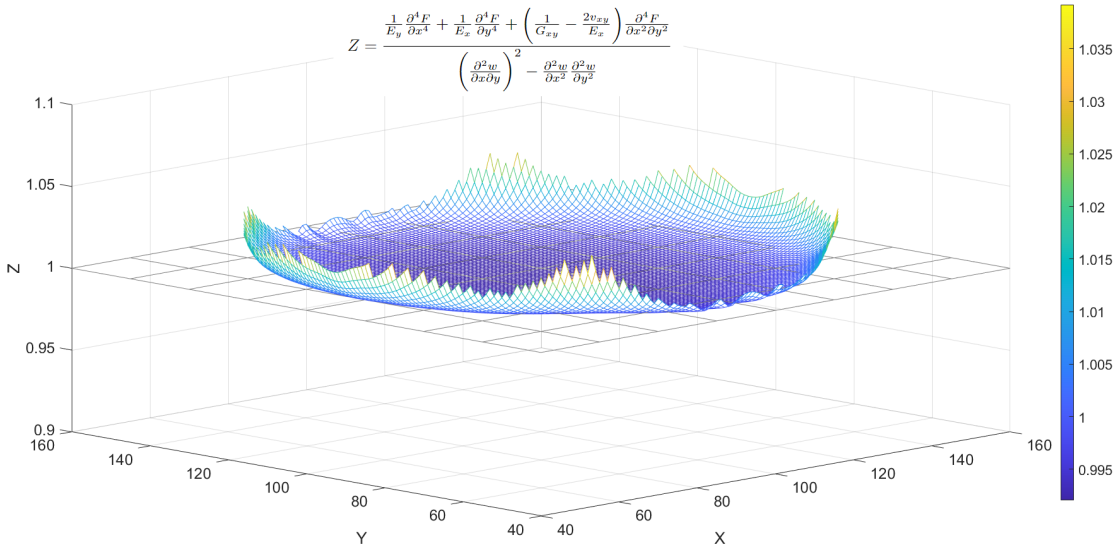

Figure 7: Quotient of the left and right sides of eq. 19 evaluated at simulated data and model inputs in the middle of the plate.

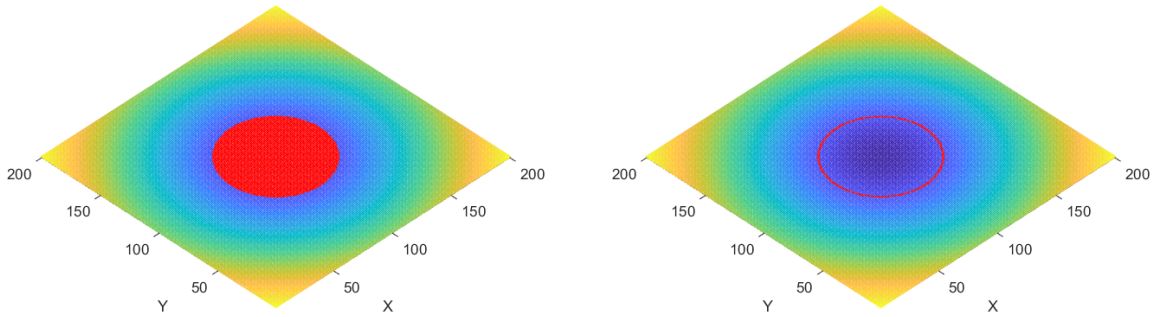

(a) Circular

(b) Ring-shaped

Figure 8: An example of domains (red) for calculating the plate's bending stiffnesses plotted over the simulated plate's deflection data w.

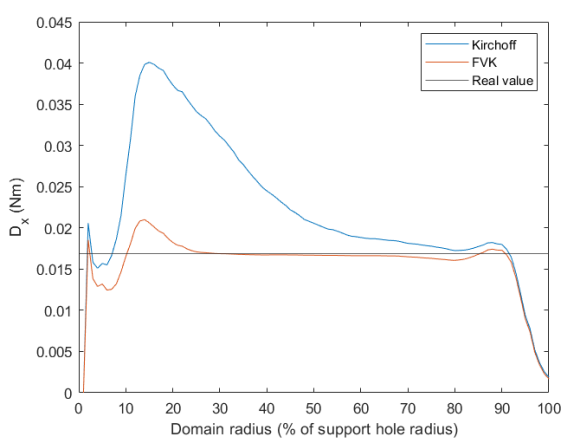

(a) D_x

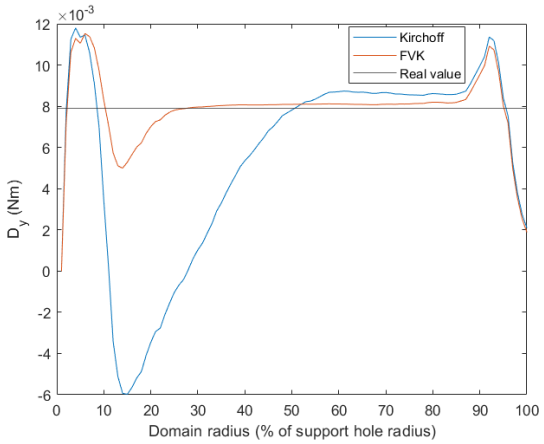

(b) D_y

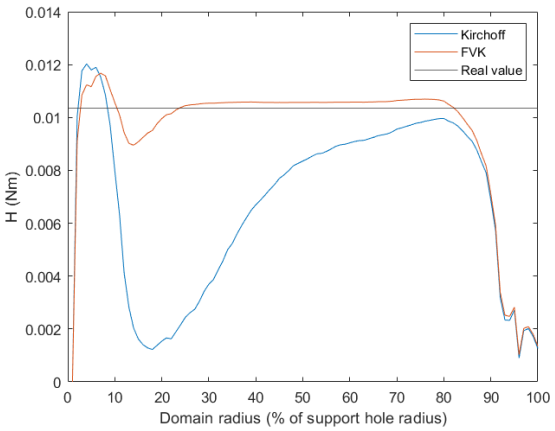

(c) H

Figure 9: Reverse-engineered plate's bending stiffnesses according to Kirchhoff and FVK equations using circular domains

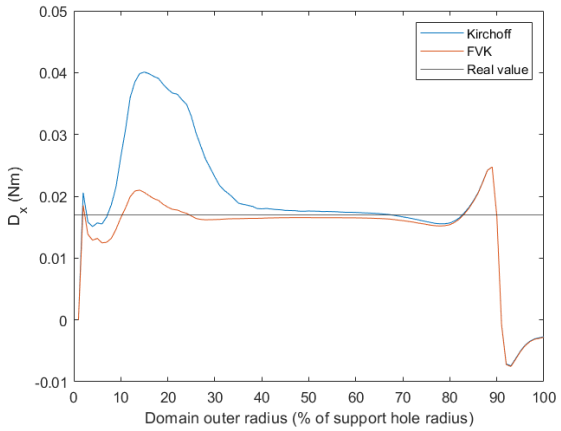

(a) D_x

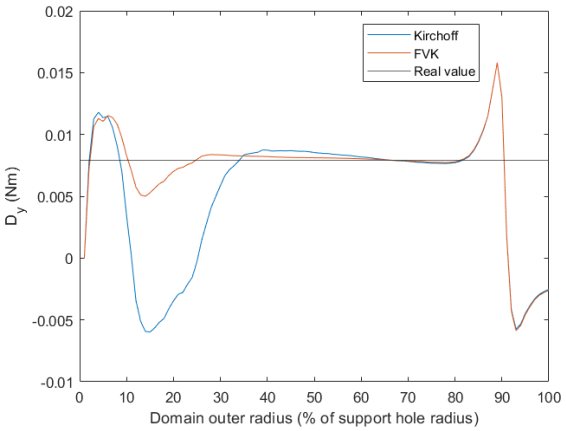

(b) D_y

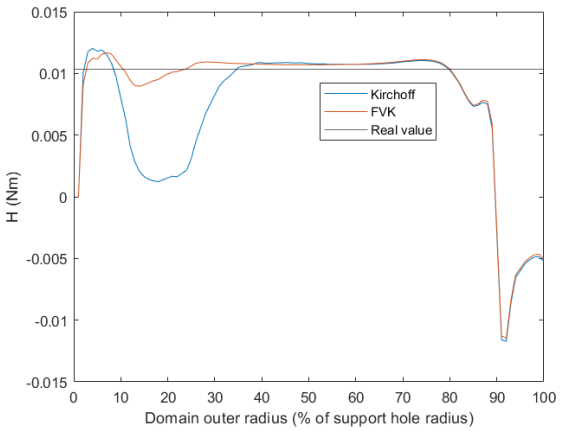

(c) H

Figure 10: Reverse-engineered plate's bending stiffnesses according to Kirchhoff and FVK equations using ring-shaped domains

that are not due to the suction load at the support plate. Moreover, the sheet in the real application is not static, but moving axially.

The results show that the FVK plate equation predicts the (FE-simulated) deflection of the plate accurately. The plate's bending stiffnesses can also be solved from the FVK equation with the additional assumption that the stresses are also known a priori. This is not the case in the real-life application.

Possible hypothesized solutions for future work that approximate the stress fields while simultaneously solving the plate's bending stiffnesses include for example solving for the stress function F from the known deflection w using Navier-type formulation similarly to Wang [18]. Another approach is to parametrize the stress fields and fit for the required parameters simultaneously with the plate's bending stiffnesses.

Most of the calculations of the material parameters used data from the center of the plate, where the deflections are large and the Kirchhoff equation is not valid. If this data is rejected, i.e., using only data points collected far from the center and far from the contact forces, Kirchhoff equation can be used to solve for the material parameter values at suitable accuracy. This is seen in Figure 10, where the Kirchhoff equation and FVK equation agree for a certain range of radii. The applicable data usage domain is much smaller in this case, which may cause problems in the least squares solution of the resulting system of linear equations when measurement noise, model inaccuracies and other disturbances are present. Very near or exactly at the edges the plate presumption (basically the form 11) is not precise and deformation in thickness direction plays a role (in real w-data). This is seen by the peak values in the calculated load in Figures 5 and 6. A chamfered edge in the support plate was also tested, but this did not remove the peak values, but some local smoothing in the values was observed. Moreover, for real materials (Table 1), $\nu_{xy} = 0.15$, but $\nu_{yx} = 0.07$ (according to equation (10)), which shows that the presumed Poisson's effect in the plane of paperboard should be highly dependent on the direction of load at the neutral plane.

Conclusions

A FE-model of a novel method for measuring the bending stiffness of paperboard was created. The FE-simulated data was used to study the validity of the Kirchhoff plate equation that is currently applied in the reverse-method. It was found that this plate equation is not sufficient for describing the larger deflections occurring in the FE-model. The Kirchhoff equation was able to solve for the FE-modeled plate's bending stiffness using the reverse-method, but only with input deflection data collected only in regions of small deflection.

The Föppl–von Kármán plate equation was in close agreement with the results and inputs of the FE-model, but required the additional knowledge of the membrane stresses in the mid-surface of the plate. This equation was successfully applied in solving the plate's bending stiffness from a broader region of data points than the Kirchhoff equation using the reverse-method. The relative error in the middle of the plate was 0.5% for the FVK plate model and 9.8% for the Kirchhoff plate model, when comparing the loads calculated from the FE-simulated data using the respective plate models with the load (-1000 Pa) used in the FE-model.

References

[1] G.A Baum. Elastic properties, paper quality, and process control *Appita journal*, 40(4):288–294, 1987.

[2] K. Bhaskar. Plates : theories and applications Wiley, New Delhi, India, 2014.

[3] P.G. Ciarlet. Plates and Junctions in Elastic Multi-structures: An Asymptotic Analysis Masson, New York, 1990.

[4] A. Föppl. Vorlesungen über technische Mechanik. Druck und Verlag von B.G. Teubner, 1907. https://archive.org/details/vorlesungenbert25fpgoog/mode/2up

[5] T. Garbowski and G. Maier and G. Novati. On calibration of orthotropic elastic-plastic constitutive models for paper foils by biaxial tests and inverse analyses. Springer-Verlag, Berlin, 2012.

[6] G. Hakim and H. Abramovich. Large Deflections of Thin-Walled Plates under Transverse Loading. *Materials*, 15(4):1577,2022. https://dx.doi.org/10.3390/ma15041577

[7] K. Hashiguchi and Y. Yamakawa. Introduction to finite strain theory for continuum elasto-plasticity. Wiley, Chichester, West Sussek, U.K, 2012–2013.

[8] A. Karakoç and E. Hiltunen and J. Paltakari. Geometrical and spatial effects on fiber network connectivity. *Composite structures*, 168:335–344, 2017. https://dx.doi.org/10.1016/j.compstruct.2017.02.062

[9] T. von Kármán. Festigkeitsprobleme im Maschinenbau. In: Encyklopädie der mathematischen Wissenschaften. Druck und Verlag von B.G. Teubner, Leipzig, 1907–1914. https://archive.org/details/p4encyklopdieder04akaduoft/page/314/mode/2up

[10] A.D. Lee and P.Shepherd and M.C. Evernden. Large deflections in thin rectangular plates subjected to uniform load: Pitfalls in the application of analytical methods. *Structures*, 27:1419–1432, 2020. https://dx.doi.org/10.1016/j.istruc.2020.06.029

[11] K. Marynowski. Dynamics of the axially moving orthotropic web. Springer, Berlin, 2008.

[12] P. Mäkelä and S. Östlund. Orthotropic elastic-plastic material model for paper materials. *International journal of solids and structures*, 40(21):5599–5620, 2003. https://dx.doi.org/10.1016/S0020-7683(03)00318-4

[13] K. Niskanen. Papermaking science and technology. Book 16, Paper Physics Finnish Paper Engineers' Association/Paperi ja Puu Oy, Helsinki, 2008

[14] M. Salo and A-L. Erkkilä and M. Vilkko and M. Kanerva. Paper bending stiffness and web tension measurement from a running web using a vacuum and computer imaging. *TAPPI J.*, 22(5):346, 2023. https://dx.doi.org/10.32964/TJ22.5.344

[15] M. Salo and J. Jokinen and M. Vilkko and M. Kanerva. Plate Bending Models for Paper Manufacturing Processes and Comparisons to Simulations with Finite Element Methods. *IFAC-PapersOnLine*, 56(2):11106–11110, 2023. https://dx.doi.org/10.1016/j.ifacol.2023.10.821

[16] S. Timoshenko and S. Woinowsky-Krieger. Theory of plates and shells. McGraw-Hill, New York, 1959.

[17] C. M. Wang and J.N. Reddy and K.H. Lee. Shear deformable beams and plates relationships with classical solutions. Elsevier, Amsterdam, 2000.

[18] D. Wang and A.I. El-Sheikh. Large-Deflection Mathematical Analysis of Rectangular Plates. *Journal of engineering mechanics*, 131(8):809–821, 2005. https://dx.doi.org/10.1061/(ASCE)0733-9399(2005)131:8(809)

Mikko Salo, Mikko Kanerva
Tampere University
Korkeakoulunkatu 6, 33720 Tampere, Finland
mikko.salo@tuni.fi, mikko.kanerva@tuni.fi

Jarno Jokinen, Matti Vilkko
Tampere University
Korkeakoulunkatu 6, 33720 Tampere, Finland
jarno.jokinen@tuni.fi, matti.vilkko@tuni.fi